Available online at www.sciencedirect.com

ScienceDirect

Solar Energy 99 (2014) 246–258

SOLAR ENERGY

www.elsevier.com/locate/solener

Verification of the SUNY direct normal irradiance model with ground measurements

Lukas Nonnenmacher, Amanpreet Kaur, Carlos F.M. Coimbra *

Department of Mechanical and Aerospace Engineering, Jacobs School of Engineering, Center for Renewable Resource Integration and Center for Energy Research, University of California, San Diego, 9500 Gilman Drive, La Jolla, CA 92093, USA

Received 3 July 2013; received in revised form 13 November 2013; accepted 14 November 2013
Available online 14 December 2013

Communicated by: Associate Editor Dr. Frank Vignola

Abstract

The accurate assessment of the Direct Normal Irradiance (DNI) component of the solar resource is notoriously difficult due to the higher cost of DNI instrumentation and the much higher requirements on proper maintenance of such instruments. Nonetheless, DNI is the only component relevant to all concentrated power technologies. The evaluation of location-specific DNI variability is of current interest to the renewable energy sector due to the steep ramp rates associated with cloud effects. The present work shows the ability of the SUNY satellite-to-irradiance model in capturing the magnitude and variability of DNI when compared with high quality ground measurements. Long-term ground DNI data is compared against concurrent SUNY DNI values after an extensive data quality control. Redundant measurements at one location enables quantification of the error in the semi-automatic irradiance data quality control. This study demonstrates the general accuracy of SUNY data and quantifies the error in assessing the magnitude and variability of DNI for several different microclimates in California. A location dependent mean bias error of -6.39% to 14.21% with a correlation coefficient (ρ) ranging from $\rho = 0.90$ to $\rho = 0.95$ is registered for long-term averages of the SUNY DNI data. Our findings indicate that the SUNY data is a valuable tool to access the DNI variability on a 30-min temporal resolution although an overestimation of small fluctuations at some locations exists. A method to correct for this overestimation of low magnitude variability is described. Overall, the SUNY data is especially important with regards to a lack of high quality ground measured DNI data and the costs associated with maintaining networks of solar instruments. However, a comparison of variability events and Variability Index (VI) on 1-min resolution to 30-min resolution data reveals that the 30-min averages obscure large shares of frequency and amplitude of DNI variability. Values of VI_{30min} that are more than six times smaller than VI_{1min} can be found within the same data sets.

Keywords: SUNY model; DNI validation; Variability index; DNI variability; Solar irradiance variability; Short-term variability

1. Introduction

Solar power generation has experienced remarkable growth in capacity and market share within the last decade. Solar energy is a promising renewable energy resource and is likely to become an important component in the energy portfolio of more sustainable societies. Solar energy power plants are designed, sized and optimized based on estimations of the solar resource at the site of deployment. A common approach to solar resource assessment concerns ground-based measurements. However, in situ measurements are costly and sensors are difficult to maintain, especially at remote locations. The inherent shortcomings of ground-based assessment motivated the development of several remote-sensing techniques to model solar irradiance at the ground level. Several methods based on satellite imagery have been developed in the past, including the

* Corresponding author. Tel.: +1 858 534 4285; fax: +1 858 534 7599.
E-mail address: ccoimbra@ucsd.edu (C.F.M. Coimbra).

0038-092X/$ - see front matter © 2013 Elsevier Ltd. All rights reserved.
http://dx.doi.org/10.1016/j.solener.2013.11.010

Heliosat Model, BRASIL-SR Model, DLR-SOLEMI Method and the SUNY model (Cano et al., 1986; Pereira et al., 2000; Schillings et al., 2004; Perez et al., 2002). These different models are based on different characteristics of geostationary satellites covering different regions on the globe. All these models are cognate and only take different technical specifications of the satellites into account to fine-tune the irradiance models. North America is covered remotely by the GOES-West and GOES-East satellite series. The SUNY model has been developed as the satellite-to-irradiance model for these satellites. This model estimates the Global Horizontal Irradiance (GHI) component based on observed cloud reflectivity and atmospheric conditions. The Direct Normal Irradiance (DNI) is also derived from cloud reflectivity with additional inputs like the Aerosol Optical Depth (AOD), sun elevation, as well as ozone and water vapor concentration data. The Diffuse Horizontal Irradiance (DHI) can also be derived using the SUNY model.

Since ground-based GHI measurements are more available than DNI ones, a recent study focused on data reliability and accuracy of GHI (Nottrott and Kleissl, 2010). In contrast, much fewer studies on the performance of the SUNY model for DNI have been conducted before, particularly regarding variability. The importance of reliable DNI data is evident in California because of its potential for Concentrated Solar Power (CSP) and the proximity of vast areas with high DNI potential to population centers (Stoddard et al., 2006).

The goal of this study is to investigate the performance of the SUNY model in providing valid DNI data and modeling solar variability for given locations. A more detailed quantification of solar variability became more important in recent years due to its significance to grid integration at higher penetration levels, e.g. design of smart inverters, transmission analysis as well as the sizing of ancillary and spinning reserves (Pedro and Coimbra, 2012; Hoff and Perez, 2012; Marquez and Coimbra, 2013a; Bosch et al., 2013). Additionally, the performance and evaluation of solar forecasting technologies are strongly dependent on local solar variability (Marquez and Coimbra, 2013b).

2. Data

2.1. Ground-truth measurements

Data quality control is critical to this study since a comprehensive analysis of the SUNY model performance requires a high level of sensitivity. Therefore, strict data quality metrics were applied throughout the experiments. Four different solar observatories were used in this study. Data points from all 4 independent locations were flagged and removed from this study if either consistency or accuracy were considered compromised. One of the locations (Merced) was used as reference, where high-quality redundant measurements of DNI were collected using several independent instruments. The data assessment and quality control procedure are described in the following sub-sections. Ground-data sets were collected at much higher sampling rates than provided by the SUNY model. Therefore, half-hourly averages of ground measurements have been calculated for the ground-data after the quality control process. For the variability analysis, values from the 1-min data sets were used in addition to the 30-min averages.

2.2. Merced

The Merced solar observatory is located in the University of California (UC), Merced campus (longitude: 37.36; latitude: −120.42). The Köppen climate classification scheme describes the climate as *Csa* (main climate $C =$ warm, precipitation $s =$ steppe and temperature $a =$ hot summer) based on Kottek et al. (2006). These climate conditions are characterized by hot, dry summers and wet, cold winters. Merced is located close to the geodesic center of California. A common weather phenomenon in this area is the occurrence of tule fog, a dense formation of ground fog that is observed normally between November and April and that causes significant ground cooling and drizzling conditions.

Data sets were collected from April 2010 until May 2012 by a setup of two Eppley Precision Spectral Pyranometers (PSP) and an Eppley Normal Incidence Pyrheliometer (NIP). One pyranometer has been used to measure GHI. The second pyranometer has been mounted on an Eppley Tracker (Model SMT-3) with a shade disk kit to measure DHI. The same tracker carried the NIP to measure DNI. Data sets were logged with a Campbell Scientific CR-1000 data-logger as 30-s average values. The calculated system accuracy for each component of this setup is $\pm 1.6\%$ given perfect alignment and cleanliness (Campbell Scientific, Inc., 2001).

Additionally to the Eppley setup, a Multi-Filter Rotating Shadowband Radiometer (MFR-7) manufactured by Yankee Environmental Systems, Inc., has been deployed in Merced from March 2011 until May 2012. The MFR-7 is a field instrument that simultaneously measures global, diffuse, and direct normal components of spectral solar irradiance (Yankee Environmental Systems, Inc., 2004, 2010). The basic idea of a shadow band irradiance instruments is the cyclical shading of a pyranometer via a shadow band to access diffuse and GHI with the same sensor. The relation between solar irradiance components can be approximately calculated by:

$$GHI = DNI \cdot \cos(\theta) + DHI, \quad (1)$$

where θ indicates the solar altitude. This equation is only an approximation; however, corrections are automatically applied by the proprietary software developed for this instrument for increased accuracy and consistency. The general error of this kind of measurement devices is below 5% for 0–80° Solar Zenith Angles (SZA) and below 1% with corrections applied (Yankee Environmental Systems,

Inc., 2004). The MFR-7 and the Eppley setup were placed less than 5 m apart.

Besides the solar observatory, a 1-MW solar photovoltaic (PV) farm is also available on campus. The solar array consists of 4900 mono-crystalline silicon, single-axis tracking PV panels. Power output data from the solar farm were recorded as 15-min averages. To match this resolution with the SUNY data, 30-min averages were calculated.

2.3. San Diego

The San Diego DNI observatory is located on the main campus of the University of California San Diego in La Jolla, CA. Data collection started on March of 2012. An MFR-7 was used for this location in the present work. The climate in La Jolla can be described as semi-arid whereas large differences on short distances occur due to the topography of the coastal region, which leads to distinct microclimates in close proximity. The sensors are located within 2 km of the coastline, and on about 100 m elevation above mean sea level. Therefore, they lie well within the region influenced by coastal marine layer clouds. Under certain conditions, these marine layer clouds form over the Pacific Ocean and advect onshore, where they can remain for days, a distinctive feature of the La Jolla region from May through August. Based on the Köppen climate classification scheme this location is referred to as *BSk* (B = arid, S = steppe, k = cold arid) or *Csa*. The San Diego solar observatory is located on the rooftop of the EBU-II building (longitude: 32.88; latitude: −117.23). At this site, some shading occurs during certain periods of the year. The days with shading effects have been removed entirely from the analysis. The MFR-7 has been checked for alignment and cleanliness several times per week.

2.4. Davis

Data sets at the location in Davis, Yolo County, California, have been acquired with an MFR-7 (longitude: 38.53; latitude: −121.78). For this study, data was collected from May 2011 until September 2012. Located in the northern portion of the Central Valley of California, the climate in Davis is similar to Merced (also characterized as *Csa* on the Köppen scheme). Davis is a remote location with no on-site staff, therefore we expect soiling effects over time.

2.5. Berkeley

The Berkeley solar observatory is located in the University of California, Berkeley campus on top of a building (longitude: 37.88; latitude: −122.26). The climate is often referred to as *Csb* on the Köppen scheme (C = warm temperature, S = steppe, b = warm summer). However, summers tend to be cooler than for typical Mediterranean climate due to the closeness to the San Francisco Bay. Additionally, the proximity to the ocean causes frequent coastal fog and light rain (see, e.g. (Gilliam, 2002) for more details). As the other locations, the Berkeley observatory is also equipped with an MFR-7. Data collection at this location started in May 2011. Although only 90 km apart, ground irradiance at Berkeley differs substantially from the ground irradiance at Davis. Due to suspected misalignment of the Berkeley MFR-7, data from 01 August 2011 to 04 September 2011 have been removed from this analysis.

2.6. SUNY data

Data for this study was provided by SolarAnywhere® for all of California based on the improved SUNY v2.0 model with corrections for high albedo conditions, enhanced resolution – 1 km; 30-min – as gridded data. Time series for the locations mentioned above have been extracted by taking the data of the pixel representing the area on the ground that includes the sensor for the ground-truth measurements. For this study, the SUNY data was available from January 2011 until September 2012.

3. Data quality control

3.1. General data-quality criteria

3.1.1. Operational errors

Quality Control (QC) for solar irradiance has been discussed in-depth by several authors. Younes et al. (2005) identified the following sources that introduce errors into solar radiation measurements: (1) cosine response of the sensor, (2) azimuth response of the sensor, (3) temperature response of the sensor, (4) spectral selectivity, (5) stability, (6) non-linearity of the sensor response, (7) shading band or kit misalignment and (8) dark offset long wave radiation error. All of these errors are addressed and minimized by the design of the measurement instruments. Younes et al. (2005) additionally identified the most common operation-related problems and errors as: (1) complete or partial shade-ring misalignment, (2) dust, snow, dew, water-droplets, bird droppings, etc., (3) incorrect sensor leveling, (4) shading, (5) electric fields of cables in the vicinity, (6) mechanical loading of cables, (7) orientation and/or improper screening of the vertical sensors from ground-reflected radiation and (8) station shut-down. The likelihood of occurrence of any of these disturbances have been minimized by a careful installation at all the locations and a regular maintenance. To address the well known error associated with the cosine response of the sensors and to exclude night values from the analysis, data collected during times when the solar elevation was below 5° have been excluded.

3.1.2. Post-measurement quality control

In addition to these pre-measurement error minimization procedures, a post-measurement quality control is necessary in order to exclude compromised measurements.

Two methods are used here: the ground-truth assessment with redundant DNI measurements in Merced, and a semi-automatic QC methodology proposed by Journe and Bertrand (2011).

3.1.3. Ground-truth assessment with redundant measurements

To ensure the highest data quality, the values measured with the Eppley instruments were compared with the measurements from the MFR-7. Measurements that showed differences in half hourly averaged values larger than 5% have been flagged and excluded from this study. 5% was chosen due to the 2.6% error as the additive error bars for the NIP and for the MFR-7 instruments plus a systematic bias of 2.4% to allow for short-term shading, horizontal misalignment or error due to spatial distance and soiling effects. The scatter plot of the ground DNI data for Merced, used in this study is shown in Fig. 1 with grey markers and is combined with the SUNY DNI data for Merced in the same plot. We consider the strongly redundant data sets as ground-truth measurements.

3.1.4. Semi-automatic quality control

Since the Merced observatory is the reference location with a long period of redundant measurements, the same type of correlation between ground measurements cannot be used in the quality control procedure for the other solar observatories. (Journe and Bertrand, 2011) proposed various procedures for post-measurement data quality control not based on redundant measurements. These procedures include physical threshold tests, step, persistence, quality envelope, spatial consistency, and sunshine tests. When applicable, these tests were implemented into a post-measurement data quality control algorithm and have been applied here. Several tests have not been used because they addressed problems that did not apply to our ground measurements (e.g. to detect snow cover events). The issues shown below based on the characteristics of the instruments have been addressed manually before application of the quality control algorithm.

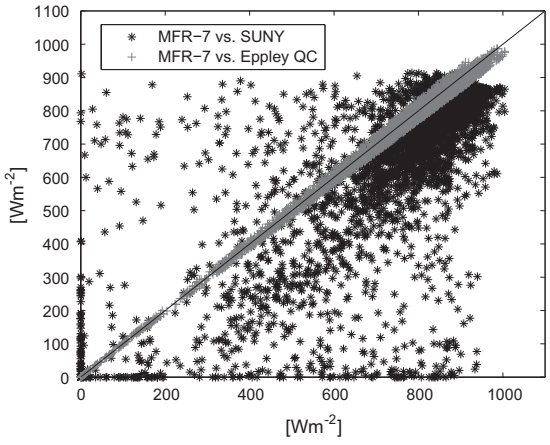

Fig. 1. Scatter plot of MFR-7 ground-truth data versus SUNY-modeled DNI data for the quality controlled data set in Merced. Ground values with a difference larger than 5% of MFR-7 and Eppley setup measurements have been removed from the analysis. The black diagonal line has been added to show the 1:1 relationship.

3.2. Instruments

All instruments used for this study are rated as secondary standard radiometers as defined by ISO 9060 and, therefore, meet the highest standards.

3.2.1. MFR-7

The most common source of error for measurements acquired with a MFR-7 results from either shadow band malfunction or horizontal misalignment. If the shadow band does not shade the sensor correctly, the DHI is not accessed correctly which leads to an error in DNI value. Misalignment leads to a distinct rippled shape in the diurnal curve of DNI and DHI irradiance. All days in the MFR-7 data sets have been checked for misalignment manually since the rippled shape was not detected with the automatic quality assessment scripts.

3.2.2. Eppley setup

Likewise to the alignment issues that apply to the MFR-7, the most frequent source of error for the DNI measurements with a pyrheliometer relates to the precise tracking of the Sun. To automatically identify days with tracker malfunction, the measured DNI (DNI_m) has been compared to the calculated DNI (DNI_c) according to Eq. (1) solved for DNI for SZA $< 85°$ based on the measurements from the two PSPs. Days got flagged for misalignment when the difference between measured and calculated values exceeded 9.8% (summed error bars of the instruments + 5% inaccuracy threshold due to the model from Eq. (1)). This was executed only to identify days with tracker misalignment. The procedure to identify ground-truth data is based on correlation and shown in Section 3.1.3. Occasionally, morning fog leads to condensed moisture on the glass of the pyrheliometer, especially at the DNI observatory in Merced which is surrounded by farmland. If that occurs, a well-defined dip is recorded in the DNI graph in the morning hours. Data impacted by condensation have been removed completely from the analysis.

3.3. Estimation of accuracy for other locations

To estimate the capabilities of the semi-automatic data quality control, the Merced data set from the MFR-7 and the Eppley setup have both been cleaned with the semi-automatic quality control described above. The statistic of the semi-automatic data quality controlled data sets are compared to the statistics of the ground-truth data set to show the capabilities of the semi-automatic data quality control (see Table 1). Especially the high cross correlation ($\rho = 0.9888$) and the low MBE and MAE indicate that the semi-automatic quality control is able to identify

Table 1
Statistics for automated quality control based on redundant measurements and the semi-automatic quality control algorithm. As expected, the automated quality control generates a higher quality data set. However the semi-automatic quality control still derives good results.

	Size of data set	Mean MFR-7 ($W\,m^{-2}$)	Mean Eppley ($W\,m^{-2}$)	MBE ($W\,m^{-2}$)	MBE (%)	MAE ($W\,m^{-2}$)	MAE (%)	RMSE ($W\,m^{-2}$)	RMSE (%)	ρ (–)	σ ($W\,m^{-2}$)	σ_p (%)
Redundant QC	4111	636.5	553.7	7.4	1.1	14.3	2.2	18.5	2.9	0.998	16.9	2.7
Semi-automatic QC	6863	490.5	449.4	13.9	2.8	28.8	5.7	50.2	10.0	0.9888	48.3	9.8

high quality data; however the error is slightly higher than with the automated quality control.

4. Methodology

4.1. Error metrics

Well-established statistical measures have been applied to compare the satellite-derived irradiance from the SUNY model with the ground measurements described above. The statistics used are the Mean Bias Error (MBE), the Mean Absolute Error (MAE), the Root Mean Square Error (RMSE), the Standard Deviation (σ) and the Correlation Coefficient (ρ) calculated as in Eqs. (3)–(6). For a more compact notation we first define ΔI as:

$$\Delta I = DNI_{measured} - DNI_{SUNY}, \tag{2}$$

it then follows:

$$MBE = \frac{1}{N}\sum_{n=1}^{N}\Delta I_n, \tag{3}$$

$$MAE = \frac{1}{N}\sum_{n=1}^{N}|\Delta I_n|, \tag{4}$$

$$RMSE = \sqrt{\left(\frac{1}{N}\sum\nolimits_{n=1}^{N}(\Delta I_n)^2\right)}, \tag{5}$$

$$\sigma = \sqrt{\frac{1}{N}\sum\nolimits_{n=1}^{N}(\Delta I_n - \overline{\Delta I})^2}), \tag{6}$$

$$\rho = \frac{\sum_{n=1}^{N}((I_{m,n} - \overline{I_m})\cdot(I_{SUNY,n} - \overline{I_{SUNY}}))}{\sqrt{\sum_{n=1}^{N}(I_{m,n} - \overline{I_m})^2 \cdot \sum_{n=1}^{N}(I_{SUNY,n} - \overline{I_{SUNY}})^2}}, \tag{7}$$

where I_m indicates the measured DNI values, I_{SUNY} indicates the DNI from the SUNY data set. Variables with an over-bar indicate the mean value of that variable. The error values given in percent in this study are always calculated with regards to the MFR-7 data values and are indicated with a subscript p. These metrics are commonly applied in the solar energy area (Djebbar et al., 2012; Vignola et al., 2007; Marquez and Coimbra, 2011).

4.2. Cloud index (kt)

To study the performance of the SUNY model for different atmospheric conditions, we related the error to the concept of cloud index (kt). kt is commonly described as:

$$kt = \frac{GHI_m}{GHI_{clear}}, \tag{8}$$

as mentioned above, GHI_m represents GHI measured with the MFR-7s (as described in Section 2.1) and GHI_{clear} refers to the expected GHI under clear-sky conditions for the same time period. Although this study validates DNI and kt is only related to GHI, the relation of error in DNI to kt is important because satellite-to-irradiance models are heavily based on the values of kt (Mueller et al., 2004; Cano et al., 1986).

4.3. Clearness index (Ci)

To relate the performance of the SUNY model in relation to the estimated clear-sky DNI, we define Ci as:

$$Ci = \frac{DNI_{measured}}{DNI_{clear}}, \tag{9}$$

where kt and Ci are values ranging between 0 and 1, where 0 indicates complete overcast conditions while 1 indicates clear skies. However, due to cloud edge effects, values higher than 1 can and do occur. In those cases, the values are set to 1. This does not interfere with the purpose of quantifying the error related to the transmissivity of the atmosphere. All clear-sky values used in this study have been calculated with the method proposed by Ineichen and Perez (models proposed and discussed in Ineichen (2006), Ineichen and Perez (2002), Gueymard (2012a)).

4.4. Solar variability

Besides high yearly average irradiance values, variability is an important factor for determining the quality of the solar resource at a certain location. Detailed information about the expected variability at a given location is also necessary to size components of solar systems accurately. Below we discuss different metrics for the assessment of variability.

4.4.1. Variability events

To quantify the capabilities of the SUNY model in providing an accurate picture of solar variability and ramp events, we first have to detrend the solar irradiance time series by removing the deterministic parts in the diurnal cycle of DNI. Therefore, we subtract the expected DNI clear-sky values from the measured and satellite-derived data and calculate the difference in DNI magnitude between two consecutive data points:

$$V_{m\backslash s,n} = (DNI_{m\backslash s} - DNI_{CS})_{n+1} - (DNI_{m\backslash s} - DNI_{CS})_n, \quad (10)$$

where $V_{m\backslash s}$ stands for the variability. The index m indicates measured and s references to satellite-derived data. Since the clear-sky model does not work perfectly, there is an error associated with this process. To take this into account, variability values $|V| < 15\ \mathrm{W\,m^{-2}}$ are removed from the variability analysis. This measure of variability is often normalized by the expected clear-sky values. However, this step is skipped to provide a more intuitive understanding of the magnitude of variability events.

To quantify solar variability in frequency and magnitude, we describe the variability (V) with a probability density function (p) for variability events (v_i) and $i = 1, \ldots, n$. Therefore, we can write:

$$p(a \leqslant v_i \leqslant b) = P(a \leqslant V \leqslant b), \quad (11)$$

where a and b represent the ramps between the limits where the number of bins has been set to $100 (N = 100)$ in our study. This analysis has been performed with a reduced but continuous data set except for data from San Diego due to the short data set at this location.

4.4.2. Variability index

(Stein et al., 2012) proposed the Variability Index (VI) as a method to quantify the variability in solar irradiance measurements. Originally, the VI was introduced for GHI measurements but it works equally well for DNI. The VI for DNI can be calculated according to the equation:

$$VI = \frac{\sum_{N=1}^{n} \sqrt{(DNI_{m\backslash s,n+1} - DNI_{m\backslash s,n})^2 + \Delta t^2}}{\sum_{N=1}^{n} \sqrt{(DNI_{CS,n+1} - DNI_{CS,n})^2 + \Delta t^2}}, \quad (12)$$

where the indices m, s and CS again relate to the source of data and Δt represents the time interval in minutes for the calculated average DNI values (30-min or 1-min as noted).

4.5. Ramp rates

In addition to the analysis of variability, it is important to relate the solar variability of a location to ramp rates in the power output of solar farms. In particular, the spatial averaging between the irradiance measurements and the size of a PV farm is of interest to plan operations and control. The PV array deployed in Merced covers an area of approximately $34{,}000\ \mathrm{m^2}$ whereas the ground measurements are point measurements (area $\sim 1\ \mathrm{cm^2}$) and the satellite data represents a vast area of approximately 1 km by 1 km or $1{,}000{,}000\ \mathrm{m^2}$. A ramp event in both power output or ground irradiance can be defined as the difference between two consecutive values (see Eq. (13)). Ramp rates in power output (Rr_{PO}) and DNI (Rr_{DNI}) are characterized as follows:

$$Rr_{PO} = P_{n+1} - P_n, \quad (13)$$

$$Rr_{DNI,m\backslash s} = DNI_{n+1,m\backslash s} - DNI_{n,m\backslash s}, \quad (14)$$

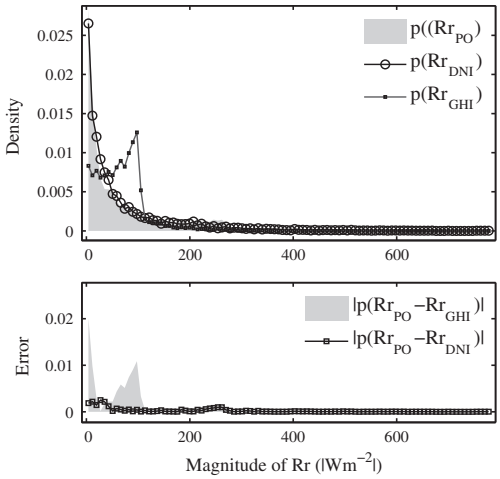

Fig. 2. Probability density function for ramp rates in DNI (Rr_{DNI}), GHI (Rr_{GHI}) and the power output of a single axis tracking PV system (Rr_{PO}). The absolute error in the probability density of ramp rates in DNI and GHI to ramps in power output is shown in the lower part of the figure. It becomes clear that the ramps of power output relate closely to ramps in DNI whereas the relation between ramps in GHI and ramps in power output is limited.

the correlation of DNI ramp rates to ramp rates in the PV array power output can be calculated as:

$$\rho_{Rr} = \frac{\sum_{n=1}^{N}((Rr_{PO,n} - \overline{Rr_{PO}}) \cdot (Rr_{m\backslash s,n} - \overline{Rr_{m\backslash s}}))}{\sqrt{\sum_{n=1}^{N}(Rr_{PO,n} - \overline{I_m})^2 \cdot \sum_{n=1}^{N}(Rr_{m\backslash s,n} - \overline{Rr_{m\backslash s}})^2}}. \quad (15)$$

The single axis tracking system enhances the impact of DNI on power output since variability and ramp rates in DNI are inherently larger than in GHI. More power output ramps of this PV system correspond closely to DNI ramps than to GHI ramp events (see Fig. 2), even though there is no concentration. This means that the PV output is dependent on both GHI and DNI depending on the mode of operation of the power output optimized tracking controls.

5. Results and discussion

5.1. Statistical results

The statistical results for the whole data set are summarized in Table 2. An MBE between -6.39% and 14.21% indicates a good estimation of the average irradiance by the SUNY model with a small location-dependent bias. For 3 of the 4 locations (Berkeley, Davis and Merced), the SUNY model tends to underestimate DNI. Overestimation of DNI occurs in San Diego. Previously, Gueymard and Wilcox (2011) reported results for sites of different characteristics than ours. Since none of the sites under study had long overcast periods or extended snow cover during winter, our results are consistent with the conclusions reached by those authors that greater difficulties for the SUNY model are only likely to occur at locations with long periods of cloud and snow cover.

Table 2
Results of the applied error metrics (Eqs.(3)–(7)) to compare DNI data measured on the ground with data from the satellite-to-irradiance model SUNY. The errors for all stations are within the same order of magnitude, however there are different characteristics for each location. All percentage values have been calculated with regards to the mean MFR-7 values. Note that the mean values of the data set are not yearly averages as the data sets for each location cover different time periods.

Location	Size of data set	Mean measured ($W\,m^{-2}$)	Mean SUNY ($W\,m^{-2}$)	MBE ($W\,m^{-2}$)	MBE (%)	MAE ($W\,m^{-2}$)	MAE (%)	RMSE ($W\,m^{-2}$)	RMSE (%)	ρ (–)	σ ($W\,m^{-2}$)	σ_p (%)
Merced	4164	636.5	569.7	66.8	10.50	97.7	15.34	137.9	21.67	0.9241	120.7	19.0
Davis	9089	499.3	428.3	71.0	14.21	108.3	21.69	151.2	30.29	0.9278	133.6	26.8
Berkeley	8861	402.5	367.2	35.2	8.75	75.1	18.67	119.9	29.79	0.9557	114.6	28.5
San Diego	3187	383.3	407.8	−24.5	−6.39	92.4	24.12	161.9	42.24	0.9063	160.0	41.7

The MAE ranging from 15.34% to 24.12% represents the magnitude of the error for each location. The task of modeling DNI is more complex than for GHI due to the larger parameter space. However, the MAE values observed here are compatible with the GHI found by Nottrott and Kleissl (2010). The RMSE for the different locations range from 21.67% to 42.24%. Previous validations found an RMSE of GHI between 20% and 35% (Nottrott and Kleissl, 2010) and an RMSE for DNI between 34% and 41% (Vignola et al., 2007; Djebbar et al., 2012) found a daily average RMSE of 52% and and RMSE of 67% for hourly DNI averages derived from remote sensing.

The range of cross correlation values between 0.9063 and 0.9557 shows good agreement between ground measurements and the SUNY data sets. A high cross correlation is especially important because of the representation of solar variability in both data sets. The error in solar variability is discussed further in Section 5.3.

Results for the error distribution with different parameters are summarized in Fig. 3 as an example for Davis. The scatter plot in Fig. 3 (left) shows the modeled DNI versus the measured DNI in Davis. The accumulation of values on the right side of the diagonal in the scatter plot suggests that the SUNY model tends to underestimate the DNI at this location. Furthermore, it is obvious that there is a wide spread of data in the scatter plot which indicates frequent random errors of different magnitude. This result is consistent with the results from the statistics in Table 2, especially the RMSE.

5.2. Error versus cloud and clearness index

The plot relating the error to cloud index in Fig. 3 (middle) shows an increasing error with decreasing cloud cover (increasing kt). Under clear-sky conditions, the expected error is supposedly smaller, however, the expected magnitude of DNI increases. Therefore, a higher range of error magnitude is possible. The clustering of values for a high cloud index ($kt > 0.7$) on the positive side is caused by the underestimation of DNI by the SUNY model at this location.

The right plot of Fig. 3 shows the magnitude of the error in $W\,m^{-2}$ related to Ci. Ci can be seen as a measure representing the clearness of the atmosphere. The maximum error for $Ci = 0$ is $-800\,W\,m^{-2}$ which occurs when the satellite model wrongly detects clear conditions when it is in fact an overcast day. However, this does not occur very often. The maximum error for $Ci = 1$ is $800\,W\,m^{-2}$ which occurs when the satellite model senses overcast sky when it is in fact clear. This extreme case also does not happen very

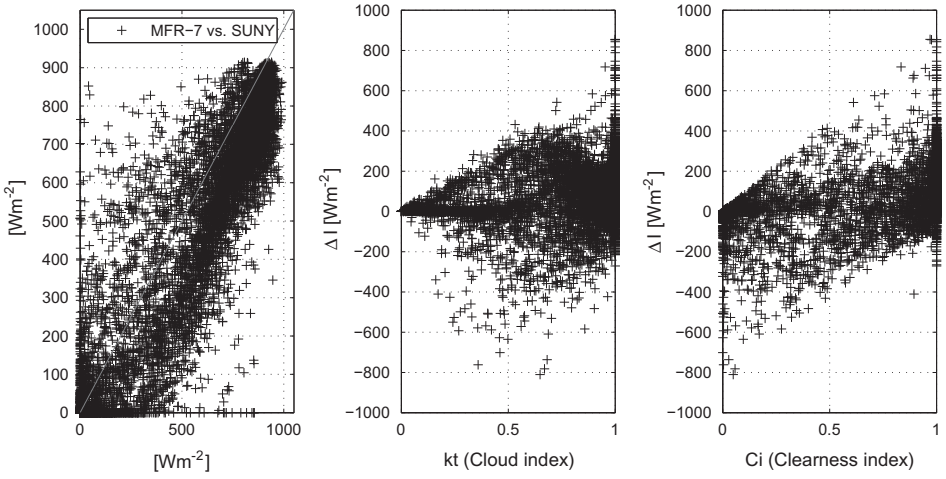

Fig. 3. The scatter plot (left) shows ground measurements versus the satellite data for the whole data set in Davis. The MBE of 14.62% leads to an accumulation of points on the right side of the diagonal. The error versus kt plot (middle) shows that the magnitude of error increases from high cloud cover to clear conditions. This can be explained by the fact that the magnitude of DNI increases and, therefore, the possible error range. The error versus Ci plot (right) leads to a rhombus shaped distribution of values. The plots are comparable to the results obtained for all the other locations.

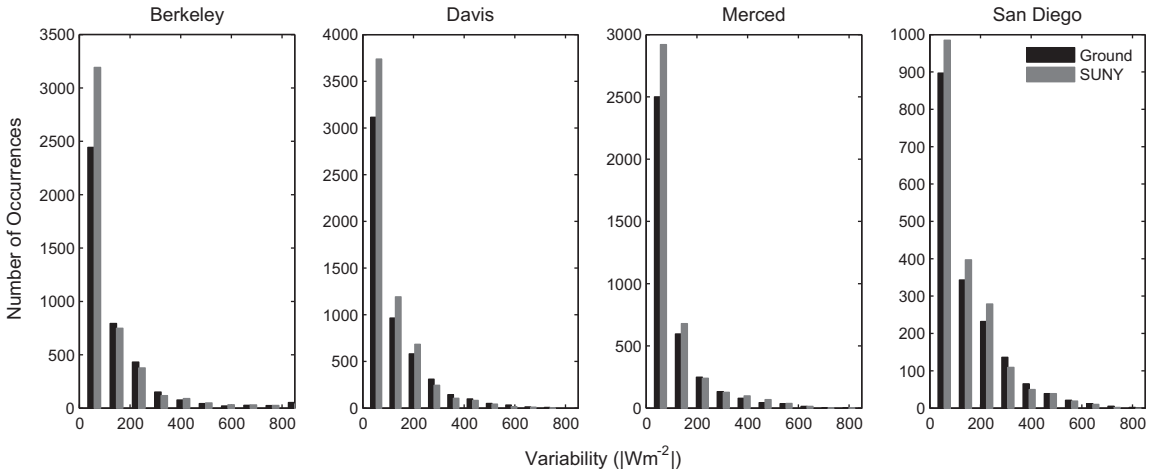

Fig. 4. Comparison between variability in ground DNI data and DNI data derived with the SUNY model for all studied locations. Both data sets follow the same trend but variability events of small magnitudes are consistently overestimated in the SUNY model. For higher ramp rates the general performance is location dependent.

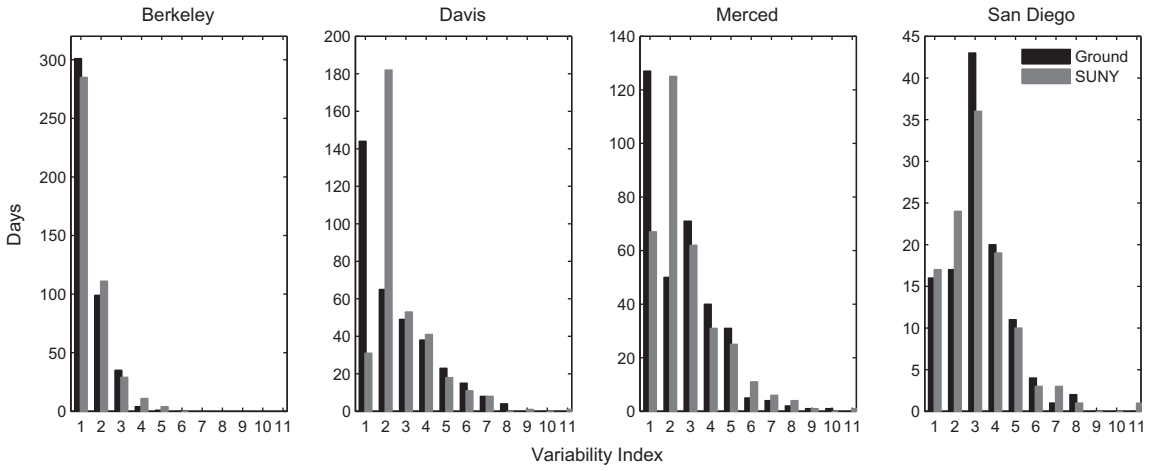

Fig. 5. Histogram of magnitude and occurrence of *VI* for four locations. It can be seen, that the variability in Berkeley is significantly lower than for the other locations. It is obvious that the SUNY model underestimates the occurrences of days with no or very low solar variability ($VI = 1$). The performance on capturing the occurrence of certain *VI* is location dependent. The error patterns described in Section 5.6.2 can explain the noticeable bias in Merced and Davis between $VI = 1$ and $VI = 2$.

often. The clustering at high *Ci* values and medium error magnitudes are due to the fact that more clear days are in the data set and a higher possible error can occur due to higher solar irradiance under clear atmospheric conditions. For Merced and Berkeley the plots show similar characteristics for the error. Taken into account that the SUNY model underestimates irradiance in San Diego the error plots are also comparable to the results shown in Fig. 3.

5.3. Error in variability

Fig. 4 shows the occurrence of variability events (*V*) in consecutive clusters of 80 W m^{-2} for all four locations, derived from the satellite-to-irradiance model and ground measurements. It is obvious that small variability events are more likely to occur. The occurrence of variability events decreases with the magnitude of the variability event. In general, the trends of the ground measurements are well reflected in the SUNY model. However, it can be seen that the SUNY model tends to overestimate the occurrence of low magnitude variability at all four locations. The extend of overestimation varies for each location (e.g. the occurrence of the lowest variability event for 15–80 W m^{-2} is overestimated in Berkeley by 30% whereas in San Diego only by 7%). The performance of the SUNY model in detecting higher ramp rates is location dependent with no obvious trend. The overestimation of variability with low magnitude can be explained with the observed error patterns discussed in Section 5.6.2.

Fig. 5 plots the occurrence of *VI* values of certain magnitude as daily values for all four locations. As a first obvious feature, it can be seen that the values achieved for *VI* in Berkeley are of significantly lower range than for the other

Table 3
Comparison of time series of daily variability indices (*VI*) calculated by MFR-7 and SUNY DNI with 30-min temporal resolution. In general, the SUNY models the average half-hourly DNI variability well. The RMSE is in the order of ~30% for all studied locations. To give an idea about the difference between ground variability derived from 1-min MFR-7 DNI measurements to the *VI* of 30-min averages, the mean and maximum of daily *VI* time series calculated with 1-min temporal resolution ground-data has been added to the table. It can be seen that the *VI* varies strongly on the different temporal resolutions.

Location	Days in data set	Mean MFR-7	Mean SUNY	max MFR-7	max SUNY	MBE	MBE_p (%)	MAE_p (%)	$RMSE_p$	ρ	σ	1-min Mean	1-min max
Berkeley	440	1.82	1.92	5.88	5.53	−0.10	−5.46	19.18	30.04	0.77	0.54	6.17	29.06
Davis	346	3.03	3.18	8.57	11.22	−0.14	−4.78	22.99	30.91	0.84	0.93	18.47	104.00
Merced	333	3.07	3.21	13.47	11.57	−0.14	−4.71	27.37	36.52	0.78	1.11	8.55	64.65
San Diego	114	3.65	3.57	8.80	11.83	0.08	2.19	20.70	30.01	0.76	1.10	14.78	67.30

locations. This can be explained by the fact that in Berkeley the sky conditions are often either clear or entirely overcast. Therefore, there is a lack of variability in irradiance as compared to the other locations. Based on the figure it can be seen that this behavior is represented well in the SUNY data with a slight underestimation of $VI = 1$ and $VI = 3$ and overestimation of $VI = 2$ and $VI > 4$. A *VI* of 1 indicates no solar variability and thus a day that is either completely overcast or continuously clear. The identification of days with no variability by SUNY data worked especially well in San Diego and Berkeley. However, in Davis and Merced a $VI = 1$ is significantly more likely to occur than modeled by SUNY. Instead, a $VI = 2$ appears considerably more often at these locations. This bias can be explained by the error patterns described in Section 5.6.2 that are especially pronounced in arid areas. In general, the occurrence of *VI* values derived by ground-data is estimated well by the SUNY model. This is also due to the fact that small modeling errors of *VI* average out in longer time series if there is no systematic bias. The statistical results from the *VI* analysis and the error between both data sets are summarized in Table 3.

Two different measures of variability have been used in this study. The results are shown in Figs. 4 and 5. The attributes of Fig. 5 are obviously different from those of Fig. 4. Both figures based on different measures of variability provide information to draw conclusions about the DNI variability at a certain location. The method of variability events shows the occurrence of ramps in $W\,m^{-2}$ and reveals the relation of occurrences of different magnitudes, while providing an intuitive way of describing variability events in $W\,m^{-2}$. In contrast to that, the *VI* is more capable of showing the variance in solar variability time series. Since the *VI* is just a number without a perceivable physical representation, this index is less intuitive but still a good method to describe and compare the variability for different locations.

5.4. Variability smoothing

The calculation of temporal averages smoothes out a large portion of the fine grain temporal variability. Fig. 6 shows diurnal cycle of DNI on a day with high solar variability on a 1-min resolution, with 30-min ground measured averages and with 30-min SUNY data. The variability derived from the DNI measurements at 1-min resolution shows, as expected, much higher frequency and amplitudes than the 30-min average data. The SUNY model values show similar characteristics concerning the occurrence of ramps; however, there are inconsistencies and a time shift when compared to ground 30-min values. The close match of VI for longer time series can be explained by the fact that small unbiased deviations are averaged out over longer periods of time. Fig. 7 shows the probability density distribution of variability for the SUNY data set, the 30-min ground measured data sets and the 1-min ground variability for all four locations. The 30-min averages of the 1-min ground DNI measurements smoothes out the frequent occurrence of large variability events. Furthermore, the maximum magnitude for variability occasionally reaches 900 $W\,m^{-2}$ on 1-min resolution, whereas the maximum magnitude of the 30-min averages only reaches 600 $W\,m^{-2}$. A comparison of the 30-min data sets shows that the variability based on the SUNY model has the same features as the ground measured variability; however, noticeable differences on a

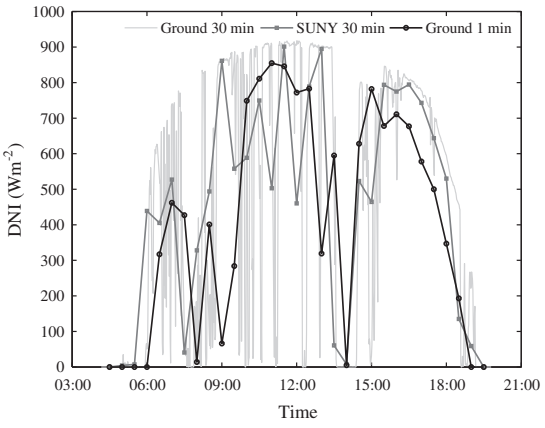

Fig. 6. Example of the diurnal irradiance of a highly variable day in Berkeley for 25 May 2012. It can be seen that the variability on a 1-min resolution is significantly higher in terms of frequency and amplitude than represented by the 30-min values. This also becomes clear by looking at VI for the different data sets: ground-data with 30-min resolution: $VI = 7.6$, SUNY data with 30-min resolution: $VI = 6.6$ and ground-data with 1-min resolution: $VI = 57.2$.

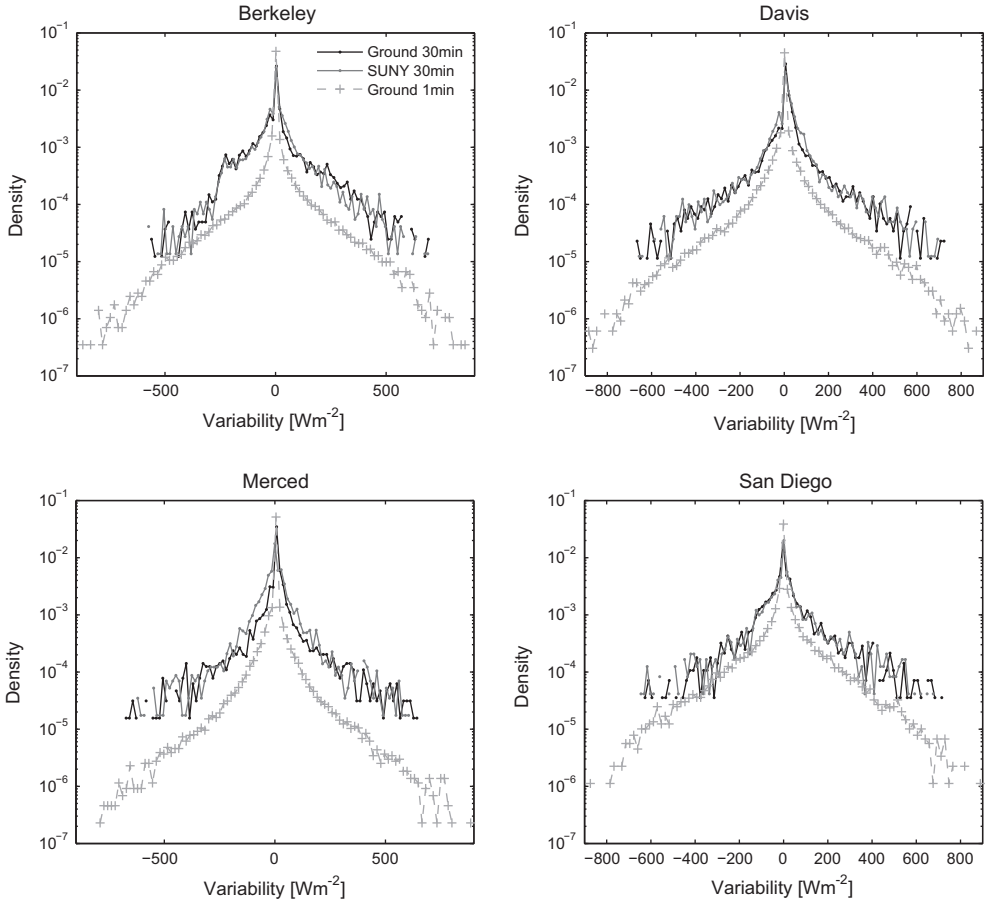

Fig. 7. Probability density function of variability for four studied locations. The 30-min solar variability is shown for ground and SUNY data sets in comparison to the ground measured variability with 1-min temporal resolution. It can be seen that the 30-min variability averages smooth out frequently occurring high solar variability events. Therefore, frequently occurring high solar variability events on the 1-min timescale are 'summarized' into more frequently occurring lower variability events as 30-min averages.

smaller scale occur. This is consistent with the behavior in Fig. 5.

5.5. Correlation of ramp rates

As stated above, the power output of a single axis tracking PV array relates to both DNI and GHI. Therefore, the correlation coefficient between ramps in PV power output data and ramps in DNI (Rr_{DNI}) is limited, and fluctuations in DNI do not necessarily cause ramps in power output (Rr_{PO}). However, large Rr_{DNI} imply strong ramps in power output from the PV array and, therefore, cause higher values of Rr_{PO}. This is illustrated in Fig. 8, where the correlation coefficient, calculated according to Eq. (15) between (Rr_{PO}) and Rr_{DNI} is shown in clusters of Rr of 20 W m^{-2}. The correlation for small and medium ramp rates ($Rr < 400$ W m^{-2}) does not exceed 0.3, which indicates only a weak linear relation. This can be explained by the fact that small Rr are often caused by advection of clouds with a low optical thickness (e.g. dispersing contrails). Under these conditions, GHI ramp events are much smaller. However, for higher ramp rates ρ_{PO} is higher and, therefore, shows a stronger linear relation between Rr_{PO} and Rr_{DNI}. Both models follow the same trend while it is not clear which DNI data set generally performs better. Therefore, we can assume that both data sets would agree in terms of resourcing for sizing the solar array.

5.6. Sources of errors and possible corrections

5.6.1. Clear-sky model

A common source of error of the SUNY model is the underlying clear-sky model. Fig. 9 shows samples for some selected clear-sky days for all four locations over time normalized to the length of the days (Sunrise= −1, Sunset= 1). It becomes clear that for Berkeley, Davis and Merced, the clear-sky model used in the SUNY model underestimates clear-sky DNI. This might be the explanation of the general trend that the SUNY model underestimates the long-term average DNI at these sites. Correcting for this by implementing more accurate clear-sky models could significantly improve the performance of the SUNY model. For San Diego, the underlying clear-sky model seems to perform better than for the other locations. However, correct modeling of clear-sky DNI is a rather complex task with inherent difficulties due to the

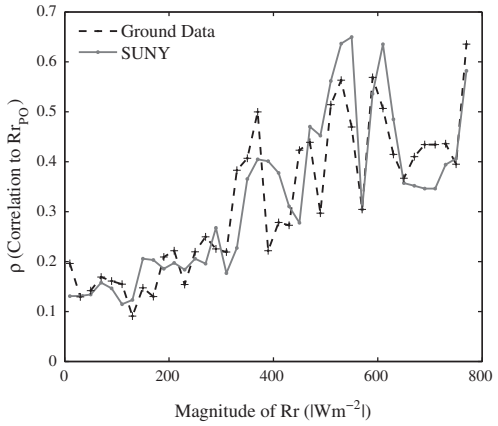

Fig. 8. Correlation coefficient (ρ_{PO}) of power output data and the two irradiance data sets versus the magnitude of ramp rates derived for ground measurements and satellite data. It can be seen that ρ is very low for small ramp rates. The correlation is generally better for higher ramps.

large number of variables determining clear-sky DNI magnitude (Louche et al., 1988; Ineichen, 2006). It is not possible to determine the AOD with satellite imagery with the required accuracy. DNI clear-sky models with accuracy comparable to high quality irradiance measurements can be achieved. These high performance clear-sky DNI models are heavily dependent on ground based measurements, especially AOD (e.g. REST2 Gueymard, 2008).

5.6.2. Observed error patterns and possible corrections

Besides the described errors due to the inaccuracies in the clear-sky model, another frequent source of error found during the analysis is most likely caused during the assessment of the ground-albedo since a certain amount of noise is introduced into the diurnal cycle. Fig. 10 shows four consecutive days of data from Merced as measured on the ground and as derived by the SUNY model as well as values calculated with the clear-sky model. It can be seen that there is a discrepancy between both data sets during midday. While the ground measurements indicate a clear day, the SUNY model assumes a certain amount of variable cloud cover or higher AOD. These patterns were found in 59 out of 339 days in Merced with a distinct accumulation between July and October. Data from the other locations showed comparable characteristics whereas the magnitude seems to be about the same in Davis and moderately weaker in Berkeley. This effect also occurs in San Diego but is less pronounced. Issues caused by certain ground-albedo effects are known (Perez et al., 2004) and can be corrected for if their properties are well defined. Previously proposed albedo corrections are already

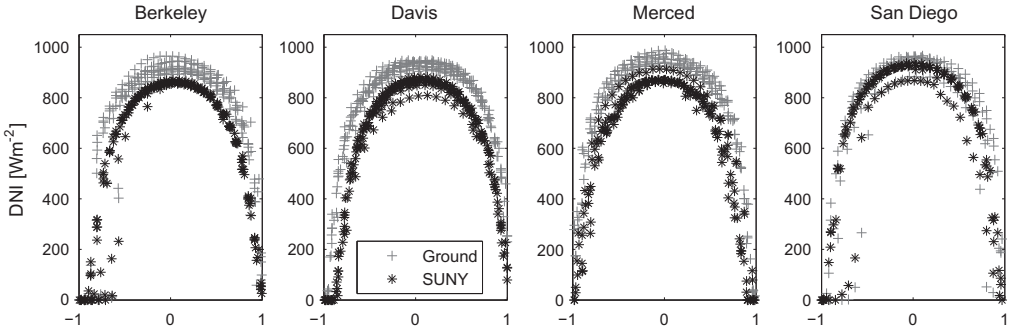

Fig. 9. The plots show days with very clear atmospheric conditions for Berkeley, Davis, Merced and San Diego (from left to right) versus normalized time. −1 indicates sunrise and 1 sunset. It becomes clear that local corrections for the clear-sky model could reduce the error significantly. Note that the plots were produced with different numbers of clear days due to availability (Berkeley: 9 days, Davis: 10 days, Merced: 8 days, San Diego: 6 days).

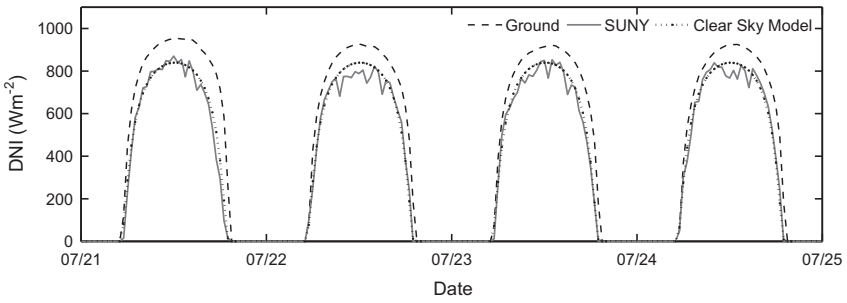

Fig. 10. The diurnal cycle of DNI on four consecutive days are shown for Merced. While the ground measurements show a clear day, the SUNY model shows variability during midday in the DNI data. This is most likely caused by an incorrect ground-albedo correction. Similar error patterns were found in the data sets of all other locations. The values of clear-sky model show the improvements after application of a clear-sky recognition system. A reliable clear-sky recognition method mitigates the overestimation of low magnitude variability (see Sections 5.3 and 5.6.2).

zimplemented in the data used. However, part of the albedo characteristics of the ground are caused by vegetation that follows a seasonal cycle with strong yearly variations and are, therefore, hard to address.

Nevertheless, this issue can be corrected for by implementing a clear-sky recognition system. One possible implementation is based on image features of processed satellite images that include an assessment of neighboring pixels in the satellite image to identify areas with no cloud cover. This method for clear-sky recognition can be optimized for the operational SUNY model. For a test data set consisting of satellite images for 107 days covering the Davis and Merced area, a simple clear-sky detection works with 87% accuracy (while 95 days have been categorized correctly as clear/overcast, 14 days have been wrongly categorized as clear, while slight cloud cover was present). Once the clear-sky areas have been identified, values can be directly drawn from the clear-sky model. In Fig. 10 the clear-sky model values show the improvements associated with the proposed clear-sky detection method. This procedure also mitigates the problem of the overestimation of small ramp rates and $VI = 2$ as described in Section 5.3.

6. Conclusions

For this study, we collected high quality DNI measurements at four locations in California (Merced, David, Berkeley and San Diego). One of these locations was used as a reference and calibration site, where measurements from two independent setups with redundant measurements of DNI were used as ground-truth measurements. Strict quality controls between data from both setups at this location have been applied to obtain very high data quality. An automatic scheme for data quality control were compared to a supervised (semi-automatic) data quality control approach for the same location in order to test the quality control methodology (Table 1). The 30-min average quality controlled ground measurements of DNI were compared to DNI data obtained with the satellite-to-irradiance model SUNY for all four locations. This comparison includes statistical measures as well as an investigation of solar energy variability in both data sets. Additionally, the correlation between ramps in both irradiance data sets to the ramp rates of a single axis, 1 MW PV array was carried out.

The main conclusions of this work are: (1) Data obtained with the SUNY model represents well the ground-truth concerning DNI variability and magnitude with the statistical characteristics shown in Table 2 for these regions where cloud cover and snow do not persist over long periods (weeks). Long periods of clouds or snow cover introduce systematic errors. The inter-annual DNI variability was not studied here (Lohmann et al., 2006; Gueymard, 2012b). (2) More accurate clear-sky models improve substantially the performance of satellite-to-irradiance models. While the ground-albedo assessment is difficult to improve, the error introduced by this process can be corrected for with a clear-sky recognition system based on satellite image features of larger areas. (3) Whereas the occurrence of small magnitude variability events is overestimated by the satellite-derived data, the frequency and amplitude of variability events are represented well by the SUNY model. The proposed correction based on improved clear-sky recognition alleviates the issue of overestimation of low magnitude fluctuations. Because most satellite-to-irradiance models are cognate, we can assume that they show similar characteristics in providing DNI variability data as shown in this study. (4) The utilization of SUNY data for sizing single axis tracking solar energy systems would result in a over- or underestimation of yearly yields depending on the location and time specific bias. However, based on the presented results concerning ramp rates in the output of a single axis tracking PV array, we conclude that the SUNY data performs well for sizing tracking solar energy systems on a 30-min resolution. (5) Considering the associated cost of maintaining DNI ground measurements, the SUNY-modeled data is a valuable resource to assess the DNI at half-hourly rates. Accurate high quality ground-data collection at high temporal resolution is still needed to assess and quantify the variability on shorter timescales, to calibrate clear-sky models and to develop short-term solar forecasting methods.

Acknowledgments

The authors gratefully acknowledge funding from the California Solar Initiative (CSI) Research, Development, Demonstration, and Deployment (RD&D) Program Grant III; and from the National Science Foundation (NSF) EECS-EPAS award No. 1201986, which is managed by Dr. Paul Werbos.

References

Bosch, J., Zheng, Y., Kleissl, J., 2013. Deriving cloud velocity from an array of solar radiation measurements. Sol. Energy 87 (0), 196–203.

Campbell Scientific, Inc., 2001. App. Note Code: 2RA-A – Eppley PSP Precision Spectral Pyranometer.

Cano, D., Monget, J., Albuisson, M., Guillard, H., Regas, N., Wald, L., 1986. A method for the determination of the global solar radiation from meteorological satellite data. Sol. Energy 37 (1), 31–39.

Djebbar, R., Morris, R., Thevenard, D., Perez, R., Schlemmer, J., 2012. Assessment of SUNY version 3 global horizontal and direct normal solar irradiance in canada. Energy Procedia 30 (0), 1274–1283.

Gilliam, H., 2002. In: Weather of the San Francisco Bay Region, vol. 63. Univ of California Press.

Gueymard, C.A., 2008. REST2: high-performance solar radiation model for cloudless-sky irradiance, illuminance, and photosynthetically active radiation validation with a benchmark dataset. Sol. Energy 82 (3), 272–285.

Gueymard, C., 2012a. Clear-sky irradiance predictions for solar resource mapping and large-scale applications: improved validation methodology and detailed performance analysis of 18 broadband radiative models. Sol. Energy 86 (8), 2145–2169.

Gueymard, C., 2012b. Temporal variability in direct and global irradiance at various time scales as affected by aerosols. Sol. Energy 86 (12), 3544–3553.

Gueymard, C., Wilcox, S.M., 2011. Assessment of spatial and temporal variability in the US solar resource from radiometric measurements and predictions from models using ground-based or satellite data. Sol. Energy 85 (5), 1068–1084.

Hoff, T.E., Perez, R., 2012. Modeling PV fleet output variability. Sol. Energy 86 (8), 2177–2189.

Ineichen, P., 2006. Comparison of eight clear sky broadband models against 16 independent data banks. Sol. Energy 80 (4), 468–478.

Ineichen, P., Perez, R., 2002. A new airmass independent formulation for the Linke turbidity coefficient. Sol. Energy 73 (3), 151–157.

Journe, M., Bertrand, C., 2011. Quality control of solar radiation data within the RMIB solar measurements network. Sol. Energy 85 (1), 72–86.

Kottek, M., Grieser, J., Beck, C., Rudolf, B., Rubel, F., 2006. World map of the Koppen–Geiger climate classification updated. Meteorol. Z. 15 (3), 259–264.

Lohmann, S., Schillings, C., Mayer, B., Meyer, R., 2006. Long-term variability of solar direct and global radiation derived from ISCCP data and comparison with reanalysis data. Sol. Energy 80 (11), 1390–1401.

Louche, A., Simonnot, G., Iqbal, M., Mermier, M., 1988. Experimental verification of some clear-sky insolation models. Sol. Energy 41 (3), 273–279.

Marquez, R., Coimbra, C.F.M., 2011. Forecasting of global and direct solar irradiance using stochastic learning methods, ground experiments and the NWS database. Sol. Energy 85 (5), 746–756.

Marquez, R., Coimbra, C.F.M., 2013a. Intra-hour DNI forecasting methodology based on cloud tracking image analysis. Sol. Energy 91, 327–336.

Marquez, R., Coimbra, C.F.M., 2013b. Proposed metric for evaluation of solar forecasting models. ASME J. Sol. Energy Eng. 135 (1), 0110161–0110169.

Mueller, R., Dagestad, K., Ineichen, P., Schroedter-Homscheidt, M., Cros, S., Dumortier, D., Kuhlemann, R., Olseth, J., Piernavieja, G., Reise, C., Wald, L., Heinemann, D., 2004. Rethinking satellite-based solar irradiance modeling: the SOLIS clear-sky module. Remote Sens. Environ. 91 (2), 160–174.

Nottrott, A., Kleissl, J., 2010. Validation of the NSRDB–SUNY global horizontal irradiance in california. Sol. Energy 84 (10), 1816–1827.

Pedro, H.T.C., Coimbra, C.F.M., 2012. Assessment of forecasting techniques for solar power production with no exogenous inputs. Sol. Energy 86 (7), 2017–2028.

Pereira, E.B., Martins, F., Abreu, S., Couto, P., Stuhlmann, R., Colle, S., 2000. Effects of burning of biomass on satellite estimations of solar irradiation in Brazil. Sol. Energy 68 (1), 91–107.

Perez, R., Ineichen, P., Moore, K., Kmiecik, M., Chain, C., George, R., Vignola, F., 2002. A new operational model for satellite-derived irradiances: description and validation. Sol. Energy 73 (5), 307–317.

Perez, R., Ineichen, P., Kmiecik, M., Moore, K., Renne, D., George, R., 2004. Producing satellite-derived irradiances in complex arid terrain. Sol. Energy 77 (4), 367–371.

Schillings, C., Mannstein, H., Meyer, R., 2004. Operational method for deriving high resolution direct normal irradiance from satellite data. Sol. Energy 76 (4), 475–484.

Stein, J., Hansen, C., Reno, M.J., 2012. The variability index: A new and novel metric for quantifying irradiance and PV output variability. In: World Renewable Energy Forum, Denver, CO.

Stoddard, L., Abiecunas, J., O'Connell, R., 2006. Economic, energy, and environmental benefits of concentrating solar power in california. Tech. rep., National Renewable Energy Laboratory, United States.

Vignola, F., Harlan, P., Perez, R., Kmiecik, M., 2007. Analysis of satellite derived beam and global solar radiation data. Sol. Energy 81 (6), 768–772.

Yankee Environmental Systems, Inc., 2004. Bulletin MFRSR-7: Multi-Filter Rotating Shadowband Radiometer Model MFR-7.

Yankee Environmental Systems, Inc., 2010. Installation and User Guide: Rotating Shadowband Radiometer Version 2.34 Rev: J.

Younes, S., Claywell, R., Muneer, T., 2005. Quality control of solar radiation data: present status and proposed new approaches. Energy 30 (9), 1533–1549.